THE UNUSUAL KUIPER BELT OBJECT 2003 SQ₃₁₇

Pedro Lacerda 1 , Andrew McNeill Astrophysics Research Centre, Queen's University Belfast, Belfast BT7 1NN

AND

Nuno Peixinho²

Center for Geophysics of the University of Coimbra Geophysical and Astronomical Observatory of the University of Coimbra Almas de Freire, 3040-004 Coimbra, Portugal Submitted to MNRAS

ABSTRACT

We report photometric observations of Kuiper belt object 2003 SQ_{317} obtained between 2011 August 21 and 2011 November 1 at the 3.58 m New Technology Telescope, La Silla. We obtained a rotational lightcurve for $2003 \, SQ_{317}$ with a large peak-to-peak photometric range, $\Delta m = 0.85 \pm 0.05$ mag, and a periodicity, $P = 7.210 \pm 0.001$ hr. We also measure a nearly neutral broadband colour $B - R = 1.05 \pm 0.18$ mag and a phase function with slope $\beta = 0.95 \pm 0.41$ mag/°. The large lightcurve range implies an extremely elongated shape for $2003 \, SQ_{317}$, possibly as a single elongated object but most simply explained as a compact binary. If modelled as a compact binary near hydrostatic equilibrium, the bulk density of $2003 \, SQ_{317}$ is near $2670 \, kg \, m^{-3}$. If $2003 \, SQ_{317}$ is instead a single, elongated object, then its equilibrium density is about $860 \, kg \, m^{-3}$. These density estimates become uncertain at the 30% level if we relax the hydrostatic assumption and account for solid, "rubble pile"-type configurations. $2003 \, SQ_{317}$ has been associated with the Haumea family based on its orbital parameters and near-infrared colour; we discuss our findings in this context. If confirmed as a close binary, $2003 \, SQ_{317}$ will be the second object of its kind identified in the Kuiper belt.

Subject headings: techniques: photometric – Kuiper belt: general – Kuiper belt objects: individual: $2003 \,\mathrm{SQ}_{317}$.

1. INTRODUCTION

Haumea is a large, triaxial KBO (semi-axes $2000 \times 1600 \times 1000$ km), with a very fast rotation (period $P \approx 3.9$ hr), a rock-rich interior (bulk density $\rho \approx 2500$ kg m⁻³) and a surface covered in high-albedo ($p \approx 0.8$), nearly pure water ice, which shows signs of variegation (Rabinowitz et al. 2006; Lacerda & Jewitt 2007; Lellouch et al. 2010; Trujillo et al. 2007; Lacerda, Jewitt & Peixinho 2008; Lacerda 2009). Haumea has two, nearly coplanar satellites with similarly icy surfaces (Brown et al. 2005; Barkume, Brown & Schaller 2006; Dumas et al. 2011).

At least 10 other KBOs have been associated with Haumea on the basis that they have similar orbital elements and water-ice-rich surfaces (Brown et al. 2007; Ragozzine & Brown 2007; Schaller & Brown 2008; Snodgrass et al. 2010; Carry et al. 2012). The origin of this so-called Haumea family is unclear. Proposed, ad-hoc scenarios include a giant impact onto the proto-Haumea (Brown et al. 2007), a gentler graze-and-merge collision (Leinhardt, Marcus & Stewart 2010) and a sequence of two collisions in which the first creates a moon which is the target of the second collision (Schlichting & Sari 2009). The first scenario is ruled out by the low velocity dispersion of the family members, while the last two possibilities are arguably improbable. Furthermore, the mass in the currently known family members and their velocity dispersion is not ideally matched by any of the

proposed scenarios (Volk & Malhotra 2012).

Snodgrass et al. (2010) noticed that one member of the Haumea family, $2003\,\mathrm{SQ_{317}}$, displayed large photometric variation, $\sim\!1$ mag peak-to-peak, in just 14 measurements. They estimated a periodicity of about 3.7 hr (or twice that) for this object. Such large variability in 200 km-scale objects often indicates extreme shapes from which useful information can be extracted (Hartmann & Cruikshank 1978; Weidenschilling 1980; Sheppard & Jewitt 2004; Lacerda & Jewitt 2007).

Here we report time-resolved, follow-up observations of $2003 \, \mathrm{SQ}_{317}$ (hereafter SQ_{317}) obtained to clarify the nature of this object and the cause for the extreme variability and to improve our understanding of the Haumea family. We find that SQ_{317} indeed has an extreme shape, most simply explained by a compact binary, although more data are needed to rule out a single, elongated shape.

2. OBSERVATIONS

We observed KBO SQ₃₁₇ using the 3.58m ESO New Technology Telescope (NTT) located at the La Silla Observatory, in Chile. The NTT was configured with the EFOSC2 instrument (Buzzoni et al. 1984; Snodgrass et al. 2008) mounted at the f/11 Nasmyth focus and equipped with a LORAL 2048×2048 CCD. We used the 2×2 binning mode bringing the effective pixel scale to 0.24''/pixel. Our observations were taken through Bessel B and R filters (ESO #639 and #642).

Each night, we collected bias calibration frames and dithered, evening and morning twilight flats through both filters. Bias and flatfield frames were grouped by

¹ lacerda.pedro@gmail.com

² Unidad de Astronomía, Universidad de Antofagasta, Avenida Angamos 601, Antofagasta, Chile

TABLE 1					
IOURNAL OF OBSERVATIONS					

Date UT	R [AU]	Δ [AU]	α [°]	Seeing ["]	Filter	Exposure [sec]	Conditions
2011 Aug 21 2011 Aug 22 2011 Aug 23 2011 Oct 30 2011 Oct 31	39.2440 39.2440 39.2440 39.2433 39.2432	38.4556 38.4452 38.4351 38.3911 38.4003	0.941 0.921 0.901 0.748	1.0 0.9 1.7 0.8	R R R,B R	600 420 420, 600 300 300	photometric photometric photometric photometric photometric
	39.2433 39.2432 39.2432	38.3911 38.4003 38.4097	0.748 0.769 0.790	0.8 0.7 0.8	R R R	300 300 300	1

NOTE. — Columns are (1) UT date of observations, (2) heliocentric distance to KBO, (3) geocentric distance to KBO, (4) solar phase angle, (5) atmospheric seeing, (6) filters used, (7) exposure times used, and (8) atmospheric conditions.

TABLE 2 PHOTOMETRY.

Date UT	$m_R \ [{ m mag}]$	$m_B \ [{ m mag}]$	B-R [mag]	$m_R(1,1,\alpha)$ [mag]
2011 Aug 21	22.44 ± 0.10	• • •		6.55 ± 0.10
2011 Aug 22	22.25 ± 0.03	• • •	• • •	6.36 ± 0.03
2011 Aug 23	22.29 ± 0.04	23.34 ± 0.18	1.05 ± 0.18	6.40 ± 0.04
2011 Oct 31	22.13 ± 0.04	• • •	• • •	6.24 ± 0.04
2011 Nov 01	22.23 ± 0.15	• • •	• • •	6.34 ± 0.15

Note. — Columns are (1) UT date of observations, (2) apparent R magnitude, (3) apparent B magnitude, (4) B-R colour, and (5) absolute R magnitude, uncorrected for illumination phase darkening. All magnitudes are at maximum lightcurve flux.

observing night and then median-combined into nightly bias, and B and R flatfields. The science images were also grouped by night and by filter and reduced (bias subtraction and division by flat field) using the IRAF ccdproc routine. The R band images suffered from slight fringing which was removed using an IRAF package optimised for EFOSC2 (Snodgrass & Carry 2013).

On photometric nights, we used observations of standard stars (MARK A1-3, 92 410, 94 401, PG2331+055B) from Landolt (1992) to achieve absolute calibration of field stars near SQ_{317} . We employed differential photometry relative to the calibrated field stars to measure the magnitude of SQ_{317} as a function of time. Uncertainty in the differential photometry of SQ_{317} (typically ± 0.05 mag) was estimated from the dispersion in the measurements relative to different stars.

Table 1 presents a journal of the observations and Table 2 lists the calibrated, apparent magnitudes at peak brightness, measured for SQ_{317} on photometric nights.

3. RESULTS

3.1. Rotational Lightcurve

Our photometry of SQ_{317} resulted in N=154 measurements over 6 nights spanning a total interval of T=1728 hours (Figure 1), The brightness of SQ_{317} varies visibly, by $\Delta m=0.85\pm0.05$ mag peak-to-peak, taking only 1.8 hours to go from minimum to maximum brightness. The full extent of this variation is seen on multiple nights.

To search for periodicity in the data we employed two methods: the Phase Dispersion Minimization (PDM; Stellingwerf 1978) and the String-Length Minimization (SLM; Dworetsky 1983). PDM minimises the ratio, Θ , between the scatter of the data phased with a trial period and that of the unphased data. The best-fit period will

result in a lightcurve with the least scatter, hence minimising Θ . SLM minimises the length of a segmented line connecting the data points phased with a trial period. Similarly to PDM, the best-fit period will result in a lightcurve with the smallest scatter around the real, periodic lightcurve and hence the shortest string length. Before running the period-search algorithms we corrected the observing times by subtracting the light-travel time from SQ_{317} to Earth for each measurement.

Figure 2 shows the PDM periodogram for lightcurve periods ranging from 3 to 11 hours. Periods outside this range resulted in larger values of Θ . Two strong PDM minima are apparent, one at $P_{1/2} \approx 3.6$ hr implying a single-peaked lightcurve with one maximum and one minimum per full rotation, and another at $P=2\times P_{1/2}\approx 7.2$ hr which folds the data onto a double-peaked lightcurve (Figure 1).

We favour the double-peaked solution, $P \approx 7.2$ hr, for three reasons. Firstly, a single-peaked lightcurve with a variation ~ 0.85 mag would have to be caused by a peculiar, large contrast, surface albedo pattern. The symmetry and regularity of the lightcurve suggest that the brightness variation is modulated instead by the elongated shape of SQ_{317} as it rotates; lightcurves produced by shape are double peaked. Secondly, the double-peaked solution produces a lightcurve with slightly asymmetric minima, seen on more than one night. The singlepeaked lightcurve minimum exhibits more scatter suggesting that it is a superposition of two different minima. Finally, the single-peaked period, $P_{1/2} \approx 3.6$ hr, would imply very fast rotation, at which SQ₃₁₇ would likely experience significant centripetal deformation for a plausible range of bulk densities and inner structures. The resulting elongated shape would produce a double-peaked lightcurve invalidating the premise that the lightcurve is

TABLE 3								
Properties	$_{\mathrm{OF}}$	$2003SQ_{317}$						

Property	Symbol	Value
Orbital semimajor axis	a	42.753 AU
Orbital eccentricity	e	0.082
Orbital inclination	i	28.6°
Equiv. diameter $(p = 0.50)$	D	$150 \mathrm{\ km}$
Equiv. diameter $(p = 0.05)$	D	$470~\mathrm{km}$
Absolute magnitude	$m_R(1,1,0)$	$5.52 \pm 0.36 \text{ mag}$
Phase function slope	β	$0.95 \pm 0.41 \text{ mag/}^{\circ}$
Lightcurve period	$\stackrel{\sim}{P}$	$7.210 \pm 0.001 \text{ hr}$
Lightcurve variation	Δm	$0.85 \pm 0.05~\mathrm{mag}$

Note. — Equivalent diameter is calculated from the measured absolute magnitude for two possible values of the geometric albedo using $D = (1329 \,\mathrm{km}) \, p^{-0.5} \, 10^{-0.2 \, m_R(1,1,0)}$

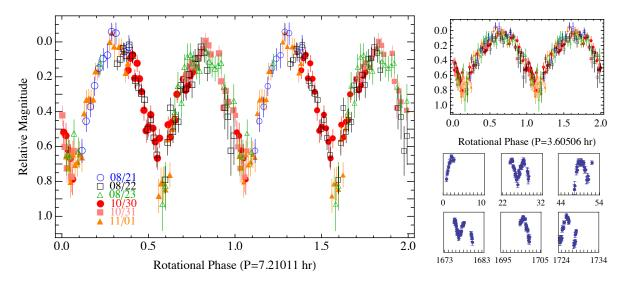


Fig. 1.— Lightcurve of SQ₃₁₇. Large panel shows data phased with the best-fit spin period P=7.21011 hr. Two full rotations are shown. Smaller panels on the right show: (top) lightcurve phased with the possible but less likely period of \sim 3.6 hr, and (bottom) measurements on each individual night with the x-axis (time) labeled in hours since MJD 55794.0 and the y-axis (unlabeled) equal to that of the figures above and to the left. The times are light-travel-time subtracted and so indicate when the light left SQ₃₁₇.

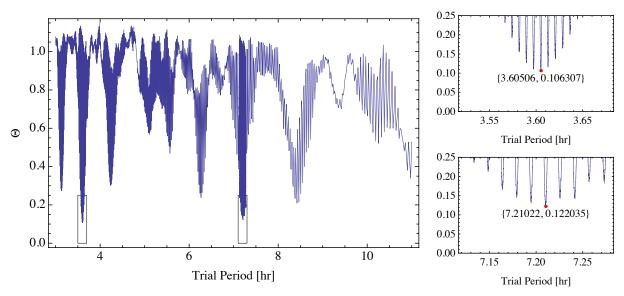


Fig. 2.— Phase dispersion minimization periodogram for the SQ_{317} data. Minima of the quantity Θ mark the most likely rotational periods. The two deepest minima are marked with boxes and enlarged on the right; the best-fit periods are shown in the insets together with the respective Θ value. Aliasing resulting from the way the data were sampled is visible in the insets.

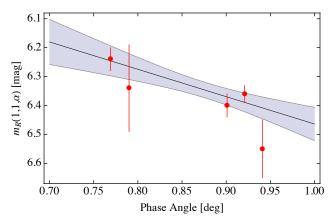


FIG. 3.— Phase curve of SQ₃₁₇ as inferred from five measurements (filled circles with error bars). A least-squares fit to the data is indicated as a black line within a shaded, 1- σ confidence region. The best fit has a slope $\beta=0.96\pm0.41~{\rm mag}/^{\circ}$ and intercept $m_R(1,1,0)=5.52\pm0.36~{\rm mag}$.

single-peaked.

High resolution analysis near the 7.2 hr lightcurve indicates a PDM minimum at $P_{\rm PDM}=7.21022$ hr, while using the SLM method, we obtained a best-fit period $P_{\rm SLM}=7.20999$ hr. We take as best-fit solution the mean of the two, P=7.21011 hr. To estimate the uncertainty in our period solution we employ (Horne & Baliunas 1986)

$$\delta f = \frac{3\pi\,\sigma_N}{2\sqrt{N}\,T\,\Delta m}$$

where δf is the uncertainty in the lightcurve frequency, σ_N is the standard deviation of the lightcurve best-fit residuals (calculated using the model shown in Figure 7), N=154 is the number of data points, T=1728 hr is the total time spanned by the observations, and $\Delta m=0.85$ mag is the lightcurve variation. The frequency uncertainty is $\delta f=0.00002$ hr⁻¹ which corresponds to an uncertainty in the spin period $\delta P=0.00103$ hr. We therefore adopt as best period $P=7.210\pm0.001$ hr.

3.2. Phase Curve

Owing to their large heliocentric distances, Kuiper belt objects are only observable from Earth at small phase angles, $\alpha < 1.5^{\circ}$. Our observations span an approximate range $0.75 < \alpha$ [°] < 0.95 and we see a trend of fainter apparent magnitude with increasing phase angle. We fitted this observed phase darkening with a weighted linear model of the form

$$m_R(1, 1, \alpha) = m_R(1, 1, 0) + \beta \alpha$$

where $m_R(1,1,0)$ is the absolute magnitude at zero phase angle and β is the linear phase curve coefficient. The fit is plotted in Figure 3 where we show apparent magnitudes at lightcurve maxima. The best-fit zeropoint and slope are $m_R(1,1,0) = 5.52 \pm 0.36$ mag and $\beta = 0.95 \pm 0.41$ mag/°. The phase function slope is steeper (although only by 2σ) than what is typically seen in other KBOs ($\beta_{\rm KBO} \sim 0.16$ mag/°; Sheppard & Jewitt 2002; Rabinowitz, Schaefer & Tourtellotte 2007) and does not follow the trend for shallower phase functions observed in other objects associated with Haumea (Rabinowitz et al. 2008). We note that the phase function found above

is consistent with the measurement $m_R = 22.05 \pm 0.02$ mag on 2008/08/30 (at phase angle $\alpha = 0.62^{\circ}$, heliocentric distance r = 39.261 AU and geocentric distance $\Delta = 38.342$ AU) by Snodgrass et al. (2010). However, because of the narrow range of phase angles sampled, the uncertainty in the phase function slope is large so we are reluctant to draw strong implications from this result.

3.3. Shape Model

The large photometric variability of SQ_{317} suggests that the object has a highly elongated, possibly binary shape. Indeed, assuming that SQ_{317} is close to hydrostatic equilibrium, its photometric range ($\Delta m = 0.85$ mag) and spin frequency ($\omega = 3.33~{\rm day}^{-1}$) place it near the threshold between the Jacobi ellipsoid and the Roche binary sequences (Leone et al. 1984; Sheppard & Jewitt 2004). To explore this issue further, we attempt to fit the lightcurve of SQ_{317} using Jacobi ellipsoid and Roche binary hydrostatic equilibrium models. The choice of models of hydrostatic equilibrium is physically based and has the benefit of allowing the density of SQ_{317} to be estimated.

We follow the procedure detailed in Lacerda & Jewitt (2007) which considers a grid of models spanning a range of Jacobi ellipsoid shapes, and Roche binary shapes, mass ratios and separations calculated using the formalism in Chandrasekhar (1963). Each model is rendered at multiple rotational phases to extract the lightcurve. Surface scattering is modelled as a linear combination of the Lambert and Lommel-Seeliger laws. The former mimics a perfectly diffuse surface and adequately describes a high-albedo, icy object displaying significant limb darkening. The latter is meant to simulate a low albedo, lunar-type surface with negligible limb darkening. These laws are linearly combined through a parameter, k, that varies between 0 (pure Lommel-Seeliger, lunar-type scattering) and 1 (pure Lambertian, icy-type scattering). The result is a collection of model lightcurves that can be compared to the one in Figure 1 to identify the bestfitting model.

As described in Lacerda & Jewitt (2007), the Jacobi ellipsoid model lightcurves are fully defined by the model's triaxial shape (semi-axes A, B, C) in terms of the axis ratios B/A and C/A, and by the coefficient k. The Roche binary lightcurves are entirely described by the binary component mass ratio q, the primary triaxial shape defined by the axes ratios B/A and C/A, the secondary shape equally defined by the triaxial axis ratios b/a and c/a, the binary separation, $d \ge 1$ (expressed in units of the sum of the primary and secondary semi-axes A + a), and the scattering parameter, k. Roche binaries are assumed to be tidally locked with the components aligned along their longest axes.

For simplicity and to keep the problem tractable we consider only models viewed equator-on. By allowing the observing geometry to vary as a free parameter we would increase the number of models that can match the lightcurve of SQ_{317} and hence the overall degeneracy of the fitting procedure. Generally, off-equator geometries lead to slightly larger mass ratio solutions, but this has been shown not to have a significant effect on the inferred bulk density (Lacerda & Jewitt 2007), arguably the most important derived property.

Each model lightcurve is adjusted (in phase and offset)

${ m TABLE} \ 4$								
Model	Fit	Parameters						

Model Type	q	d	B/A	C/A	b/a	c/a	$\rho \; [\mathrm{kg} \; \mathrm{m}^{-3}]$
Jacobi Ellipsoid Roche Binary	$0.32^{+0.08}_{-0.07}$	$1.14^{+0.14}_{-0.04}$	$\begin{array}{c} 0.55^{+0.05}_{-0.04} \\ 0.91^{+0.01}_{-0.03} \end{array}$	$0.41^{+0.02}_{-0.02} \\ 0.82^{+0.01}_{-0.02}$	$0.51^{+0.15}_{-0.07}$	$0.48^{+0.13}_{-0.07}$	$861_{-32}^{+33} \\ 2671_{-102}^{+88}$

Note. — Columns are (1) Model used to fit lightcurve, (2) component mass ratio, (3) binary separation in units of A + a, (4) and (5) primary semimajor axes, (6) and (7) secondary semimajor axes, and (8) model bulk density.

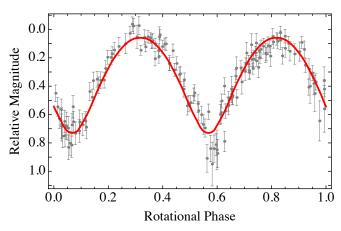


Fig. 4.— Best-fit Jacobi ellipsoid lightcurve (solid line) plotted over the lightcurve data for SQ_{317} (grey points). The corresponding Jacobi ellipsoid is shown in Figure 5.

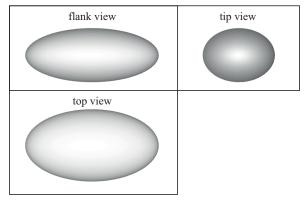


Fig. 5.— Jacobi ellipsoid model that best fits the lightcurve of SQ_{317} .

to the data using a Levenberg-Marquardt algorithm and the best-fitting one is selected using a χ^2 criterion. To explore the dependence of this procedure on the measurement uncertainties we employ a Monte Carlo approach: we generate N=371 bootstrapped instances of the lightcurve of SQ_{317} by randomising each data point within its uncertainty error bar (errors are assumed normal with standard deviation equal to the size of the error bar). Finally, we find the best (minimum χ^2) model for each bootstrapped version lightcurve and thus obtain the distribution of best-fit parameters.

Figure 4 shows the best-fitting Jacobi ellipsoid lightcurve and Figure 5 shows the corresponding model shape. The Monte Carlo distributions of best-fit parameters are shown in Figure 6. Figures 7, 8, and 9 show the best-fitting lightcurve, best model shape and parameter distributions for Roche binary models. Ta-

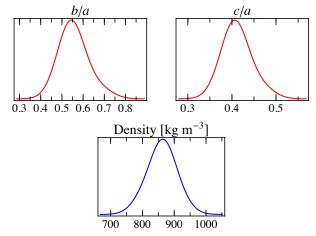


Fig. 6.— Monte Carlo distribution of Jacobi ellipsoid parameters (b/a and c/a) that fit the lightcurve of SQ_{317} . The Monte Carlo distribution of bulk density for these models is also shown.

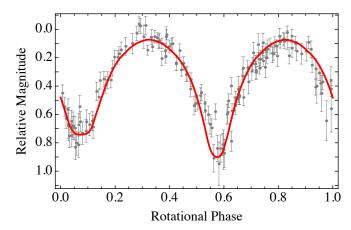


Fig. 7.— Best-fit Roche binary lightcurve (solid line) plotted over the lightcurve data for SQ_{317} (grey points). The corresponding Roche binary is shown in Figure 8.

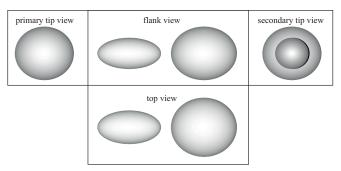


Fig. 8.— Roche binary model that best fits the lightcurve of SQ_{317} .

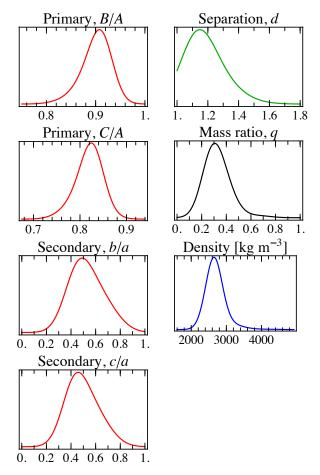


FIG. 9.— Monte Carlo distribution of Roche binary parameters (mass ratio q, binary separation d, B/A, C/A, b/a and c/a) that fit the lightcurve of SQ₃₁₇. The Monte Carlo distribution of bulk density for these models is also shown.

ble 4 summarises the best-fit parameters for each model. The Roche binary fits are generally better with a typical $\chi^2 \approx 1.62$ per degree of freedom compared to $\chi^2 \approx 1.74$ per degree of freedom for the Jacobi ellipsoid models. The Roche binary model successfully fits the different minima in the lightcurve of SQ_{317} , unlike the Jacobi ellipsoid model. The mean scattering parameter for Jacobi ellipsoid fits is k=0.1, consistent with a lowalbedo surface, while for Roche binaries we find a mean k=0.4, lending almost equal weights to (dark) lunarand (bright) icy-type terrains. Higher k values imply stronger limb darkening, which is needed to fit the different lightcurve minima.

3.4. Bulk Density

In §3.3 we found the Jacobi ellipsoid and Roche binary that best fit the lightcurve of SQ₃₁₇. Because these models assume hydrostatic equilibrium, their shapes are uniquely related to bulk density and spin period and allow us to use the latter to constrain the former. Each model shape is a function of the dimensionless parameter $\Omega^2 = \omega^2/(\pi G \rho)$ where $\omega = 2\pi/P$ is the angular rotation frequency (P is the period), G is the gravitational constant and ρ is the bulk density. For a spin period P=7.21 hr, the density is then calculated as $\rho=280/\Omega^2$ kg m⁻³.

Predictably, the two types of model imply very differ-

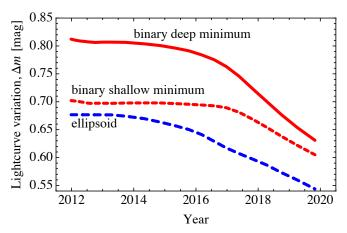


Fig. 10.— Model lightcurve variation, Δm , as a function of time for the Jacobi ellipsoid (dash-dot, blue) and the Roche binary solution. In the case of the binary model, the changes for the shallow (dashed, red) and deep (solid, red) minima are shown. The change in Δm plotted here is maximal as it assumes that the models have 90° obliquity.

ent bulk densities (Figures 6 and 9, Table 4). The Jacobi model fit yields $\Omega^2 = 0.325 \pm 0.012$ and indicates a bulk density $\rho = 860 \pm 30$ kg m⁻³, consistent with an icy composition. The Roche binary model has $\Omega^2 = 0.105 \pm 0.004$ and leads to $\rho = 2700 \pm 100$ kg m⁻³ suggesting a rock-rich bulk composition for SQ₃₁₇.

4. DISCUSSION

As the analysis in $\S 3.1$ shows, SQ_{317} oscillates in brightness by $\Delta m = 0.85 \pm 0.05$ mag, making it the second most variable KBO known, only surpassed by $2001 \, \text{QG}_{298}$ (hereafter QG_{298}) with $\Delta m = 1.14 \pm 0.04$ mag (Sheppard & Jewitt 2004). For bodies in hydrostatic equilibrium, lightcurve variation $\Delta m > 0.9$ mag can only plausibly be explained by a tidally distorted, binary shape (Weidenschilling 1980; Leone et al. 1984). That is the case of QG₂₉₈ which was successfully modelled as a Roche binary leading to an estimated bulk density near 660 kg m⁻³ (Takahashi et al. 2004; Lacerda & Jewitt 2007; Gnat & Sari 2010). The Roche binary model received further support as QG_{298} was re-observed in 2010 to show a predicted decrease in variability to $\Delta m = 0.7$ magnitudes, which allowed the obliquity of the system to be estimated at very near 90° (Lacerda 2011).

With $\Delta m = 0.85$ mag and P = 7.21 hr, SQ_{317} lies at the threshold between the Jacobi and Roche sequences (Leone et al. 1984; Sheppard & Jewitt 2004). Indeed, we find that SQ_{317} can be fitted reasonably well both by Jacobi and Roche models. However, one important feature of the lightcurve, the asymmetric lightcurve minima, is only naturally fitted by the Roche binary model. The Jacobi model misses the data points that mark the faintest point of the lightcurve (Figure 4). In theory, a special arrangement of brighter and darker surface patches could be adopted to ensure that the Jacobi model fit the fainter lightcurve minimum. However, the binary model does not require any further assumptions and thus provides a simpler explanation for the asymmetric lightcurve minima. Figure 10 plots the change in lightcurve variation, Δm , for both models. To maximise the change, we assumed the models to have 90° obliquity so that an angular displacement, ν , along the heliocentric orbit will translate into a change in aspect angle $\theta \approx \nu$ (Lacerda 2011). The two models produce slightly different behaviour and future observations may help rule out one of the solutions.

The Jacobi and Roche model solutions predict significantly different bulk densities for SQ_{317} . The former is consistent with a density around 860 kg m⁻³ which would indicate a predominantly icy interior and significant porosity. The Roche binary model implies a density close to 2670 kg m $^{-3}$, consistent with a rocky bulk composition. Densities higher than 2000 kg m⁻³ have only been measured for the larger KBOs, Eris (Brown & Schaller 2007; Sicardy et al. 2011), Pluto (Null, Owen & Synnott 1993; Buie et al. 2006), Haumea (Rabinowitz et al. 2006; Lacerda & Jewitt 2007) and Quaoar (Fornasier et al. 2013). Densities for objects with diameters similar to SQ_{317} tend to fall in the range $500 < \rho < 1000$ ${\rm kg}~{\rm m}^{-3}$ (Grundy et al. 2012; Stansberry et al. 2012) with the possible exception of (88611) Teharonhiawako with $\rho \approx 1400 \text{ kg m}^{-3}$ (Osip, Kern & Elliot 2003; Lellouch et al. 2013). If confirmed, the Roche model density of SQ_{317} would make it one of the highest density known KBOs and the densest of its size.

In a scenario in which the Haumea family was produced by a collision that ejected the volatile-rich mantle of the proto-Haumea, its members would be expected to be mainly icy in composition, with high albedo surfaces. The Jacobi model density for SQ_{317} would favour such a scenario (although the implied surface scattering is inconsistent with an icy, high albedo and high limb-darknening surface) whereas the Roche model density would be harder to explain in the context of the family. Haumea's density $\rho \approx 2600 \text{ kg m}^{-3}$ and water-ice spectrum implies a rocky core surrounded by a veneer of ice. If SQ_{317} has high-density and was produced from a collision onto Haumea then it must be a fragment from the core material.

Broadband near-infrared photometry of SQ_{317} suggests a surface rich in water ice (Snodgrass et al. 2010). Our measurements indicate a nearly solar³ surface colour $B-R=1.05\pm0.18$ mag and a steep (although poorly constrained) phase function with slope $\beta=0.95\pm0.41$ mag/°. While the visible and infrared colours of SQ_{317} match those of other members of the Haumea family, the phase function is much steeper.

The albedo of SQ_{317} is unknown. Although its surface is blue and possibly water-ice rich, these properties do not necessary imply high albedo. For instance, $2002 \,\mathrm{MS_4}$ has blue colour $(B-R\approx 1.0 \,\mathrm{mag}; \,\mathrm{Peixinho} \,\mathrm{et} \,\mathrm{al.} \,\,2012)$ but low albedo $(p_V\approx 0.05; \,\mathrm{Lellouch} \,\mathrm{et} \,\mathrm{al.} \,\,2013), \,\mathrm{and}$ Quaoar displays strong water-ice absorption (Jewitt & Luu 2004) despite its relatively dark $(p_V\approx 0.12; \,\mathrm{Lellouch} \,\mathrm{et} \,\mathrm{al.} \,\,2013)$ and red surface $(B-R\approx 1.6 \,\mathrm{mag}; \,\mathrm{Peixinho} \,\mathrm{et} \,\mathrm{al.} \,\,2012).$ Water ice has been spectroscopically detected on objects with albedos as low as $0.04, \,\mathrm{e.g.}$ Chariklo (Guilbert et al. 2009), and as high as $0.80, \,\mathrm{e.g.}$ Haumea (Trujillo et al. 2007).

The shape models and density estimates presented above assume an idealised fluid object in hydrostatic equilibrium. As a limiting case, the simplification is useful because it offers a simple and unique relation between shape, spin period and bulk density. However,

 SQ_{317} is a solid body and likely behaves differently. Holsapple (2001, 2004) have studied extensively the equilibrium configurations of rotating solid bodies—sometimes termed "rubble piles"—that possess no tensile strength but that can retain shapes bracketing the hydrostatic solution due to pressure-induced, internal friction. Similar studies were performed for Roche figures of equilibrium by Sharma (2009). The deviation from the hydrostatic equilibrium solution is usually quantified in terms of an increasing angle of friction, $0^{\circ} < \phi < 90^{\circ}$. For a positive value of ϕ , a range of bulk densities (which includes the hydrostatic equilibrium solution) is possible for an object with a given shape and spin rate.

For a plausible range of albedos, SQ_{317} has an equivalent diameter in the range 150 < D < 450 km. The giant planet icy moons in the same size range (Amalthea at Jupiter and Mimas, Phoebe and Janus at Saturn; Hyperion has chaotic rotation and is ignored) lie at the threshold between near hydrostatic shapes and slightly more irregular configurations (Thomas 2010; Castillo-Rogez et al. 2012). When approximated by triaxial ellipsoids and plotted on the diagrams of Holsapple (2001), the shapes, spins and densities of these moons are consistent with angles of friction $\phi < 5^{\circ}$ (see also Sharma 2009). Similar values of ϕ are found for most large, approximately triaxial asteroids (Sharma, Jenkins & Burns 2009). If we take our Jacobi ellipsoid solution for SQ_{317} and assume an angle of friction $\phi = 5^{\circ}$ then we find that its density should lie in the range $670 < \rho < 1100$ kg m^{-3} , i.e. a 30% departure from the idealised hydrostatic equilibrium solution. A similar uncertainty applied to the Roche binary density estimate yields a range $2050<\rho<3470~{\rm kg~m^{-3}}.$

5. SUMMARY

We present time-resolved photometric observations of Kuiper belt object $2003\,\mathrm{SQ}_{317}$ obtained in August and October 2011 to investigate its nature. Our results can be summarised as follows:

- 1. SQ_{317} exhibited a highly variable photometric lightcurve with a peak-to-peak range $\Delta m = 0.85 \pm 0.05$ magnitudes and period $P = 7.210 \pm 0.001$ hours. The object has an almost solar broadband colour $B-R=1.05\pm0.18$ mag, making it one of the bluest KBOs known. The phase function of SQ_{317} is well matched by a linear relation with intercept $m_R(1,1,0)=5.52\pm0.36$ mag and slope $\beta=0.96\pm0.41$ mag/°. This linear phase function is consistent with an earlier measurement obtained in 2008 at phase angle $\alpha=0.62^\circ$.
- 2. The lightcurve implies that SQ_{317} is highly elongated in shape. Assuming that the object is in hydrostatic equilibrium, we find that the lightcurve of SQ_{317} is best fit by a compact Roche binary model with mass ratio $q \sim 0.3$, and triaxial primary and secondary components with axes ratios $B/A \sim 0.9$, $C/A \sim 0.8$ and $b/a \sim c/a \sim 0.5$, separated by $d \sim 1.1(A+a)$. The data are also adequately fitted by a highly elongated, Jacobi triaxial ellipsoid model with axes ratios $B/A \sim 0.55$ and $C/A \sim 0.41$. Observations in this decade may be able to rule out one of the two solutions.

 $^{^3~(}B-R)_{\odot}=1.00\pm0.02$ mag (Holmberg, Flynn & Portinari 2006)

3. If $\rm SQ_{317}$ is a Roche binary then its bulk density is approximately 2670 kg $^{-3}.$ This model-dependent density implies rock-rich composition for this object. However, if SQ_{317} is a Jacobi ellipsoid we find a significantly lower density, $\rho \approx 860 \text{ kg m}^{-3} \text{ con-}$ sistent with an icy, porous interior. These density estimates become uncertain at the 30% level if we relax the hydrostatic assumption and account for

"rubble pile"-type configurations.

We thank David Jewitt for comments, and Colin Snodgrass for supplying an IRAF fringe removal routine optimised for EFOSC2. The presented data were obtained at the ESO facilities at La Silla under programmes 087.C-0980A and 088.C-0634A.

REFERENCES

Barkume K. M., Brown M. E., Schaller E. L., 2006, ApJ, 640, L87 Brown M. E., Barkume K. M., Ragozzine D., Schaller E. L., 2007, Nature, 446, 294 Brown M. E. et al., 2005, ApJ, 632, L45

Brown M. E., Schaller E. L., 2007, Science, 316, 1585

Buie M. W., Grundy W. M., Young E. F., Young L. A., Stern S. A., 2006, AJ, 132, 290

Buzzoni B. et al., 1984, The Messenger, 38, 9

Carry B., Snodgrass C., Lacerda P., Hainaut O., Dumas C., 2012, A&A, 544, A137

Castillo-Rogez J. C., Johnson T. V., Thomas P. C., Choukroun M., Matson D. L., Lunine J. I., 2012, Icarus, 219, 86

Chandrasekhar S., 1963, ApJ, 138, 1182

Dumas C., Carry B., Hestroffer D., Merlin F., 2011, A&A, 528,

Dworetsky M. M., 1983, MNRAS, 203, 917

Fornasier S. et al., 2013, A&A, 555, A15

Gnat O., Sari R., 2010, ApJ, 719, 1602

Grundy W. M. et al., 2012, Icarus, 220, 74

Guilbert A. et al., 2009, A&A, 501, 777

Hartmann W. K., Cruikshank D. P., 1978, Icarus, 36, 353

Holmberg J., Flynn C., Portinari L., 2006, MNRAS, 367, 449

Holsapple K. A., 2001, Icarus, 154, 432

Holsapple K. A., 2004, Icarus, 172, 272

Horne J. H., Baliunas S. L., 1986, ApJ, 302, 757

Jewitt D. C., Luu J., 2004, Nature, 432, 731

Lacerda P., 2009, AJ, 137, 3404

Lacerda P., 2011, AJ, 142, 90

Lacerda P., Jewitt D., Peixinho N., 2008, AJ, 135, 1749

Lacerda P., Jewitt D. C., 2007, AJ, 133, 1393

Landolt A. U., 1992, AJ, 104, 340

Leinhardt Z. M., Marcus R. A., Stewart S. T., 2010, ApJ, 714,

Lellouch E. et al., 2010, A&A, 518, L147

Lellouch E. et al., 2013, A&A (in press)

Leone G., Paolicchi P., Farinella P., Zappala V., 1984, A&A, 140,

Null G. W., Owen W. M., Synnott S. P., 1993, AJ, 105, 2319 Osip D. J., Kern S. D., Elliot J. L., 2003, Earth Moon and Planets, 92, 409

Peixinho N., Delsanti A., Guilbert-Lepoutre A., Gafeira R., Lacerda P., 2012, A&A, 546, A86

Rabinowitz D. L., Barkume K., Brown M. E., Roe H., Schwartz $\mathcal{M}.,$ Tourtellotte S., Trujillo C., 2006, ApJ, 639, 1238

Rabinowitz D. L., Schaefer B. E., Schaefer M., Tourtellotte S. W., 2008, AJ, 136, 1502

Rabinowitz D. L., Schaefer B. E., Tourtellotte S. W., 2007, AJ, 133, 26

Ragozzine D., Brown M. E., 2007, AJ, 134, 2160

Schaller E. L., Brown M. E., 2008, ApJ, 684, L107

Schlichting H. E., Sari R., 2009, ApJ, 700, 1242

Sharma I., 2009, Icarus, 200, 636 Sharma I., Jenkins J. T., Burns J. A., 2009, Icarus, 200, 304

Sheppard S. S., Jewitt D., 2004, AJ, 127, 3023

Sheppard S. S., Jewitt D. C., 2002, AJ, 124, 1757

Sicardy B. et al., 2011, Nature, 478, 493

Snodgrass C., Carry B., 2013, The Messenger, 152, 14

Snodgrass C., Carry B., Dumas C., Hainaut O., 2010, A&A, 511,

Snodgrass C., Saviane I., Monaco L., Sinclaire P., 2008, The Messenger, 132, 18

Stansberry J. A. et al., 2012, Icarus, 219, 676

Stellingwerf R. F., 1978, ApJ, 224, 953

Takahashi S., Shinokawa K., Yoshida F., Mukai T., Ip W. H., Kawabata K., 2004, Earth, Planets, and Space, 56, 997

Thomas P. C., 2010, Icarus, 208, 395

Trujillo C. A., Brown M. E., Barkume K. M., Schaller E. L.,

Rabinowitz D. L., 2007, ApJ, 655, 1172

Volk K., Malhotra R., 2012, Icarus, 221, 106

Weidenschilling S. J., 1980, Icarus, 44, 807